Dynamics of Cellulose−Water Interfaces: NMR Spin−Lattice Relaxation Times Calculated from Atomistic Computer Simulations

Malin Bergenstråhle,*,† Jakob Wohlert,† Per Tomas Larsson,‡ Karim Mazeau,§ and Lars A. Berglund†,||

KTH Department of Fibre and Polymer Technology, 10044 Stockholm, Sweden, STFI-Packforsk AB, 11486 Stockholm, Sweden, Centre de Recherches sur les Macromolécules Végétales (CERMAV-CNRS), BP53, 38041, Grenoble cedex 9, France, affiliated with Université Joseph Fourier, and member of the Institut de Chimie Moléculaire de Grenoble

Received: June 15, 2007; In Final Form: November 22, 2007

Solid-state nuclear magnetic resonance (CP/MAS ^{13}C NMR) spectroscopy has often been used to study cellulose structure, but some features of the cellulose NMR spectrum are not yet fully understood. One such feature is a doublet around 84 ppm, a signal that has been proposed to originate from C4 atoms at cellulose fibril surfaces. The two peaks yield different T_1, differing by approximately a factor of 2 at 75 MHz. In this study, we calculate T_1 from C4−H4 vector dynamics obtained from molecular dynamics computer simulations of cellulose I β−water interfacial systems. Calculated and experimentally obtained T_1 values for C4 atoms in surface chains fell within the same order of magnitude, 3−20 s. This means that the applied force field reproduces relevant surface dynamics for the cellulose−water interface sufficiently well. Furthermore, a difference in T_1 of about a factor of 2 in the range of Larmor frequencies 25−150 MHz was found for C4 atoms in chains located on top of two different crystallographic planes, namely, (110) and ($1\bar{1}0$). A previously proposed explanation that the C4 peak doublet could derive from surfaces parallel to different crystallographic planes is herewith strengthened by computationally obtained evidence. Another suggested basis for this difference is that the doublet originates from C4 atoms located in surface anhydro-glucose units with hydroxymethyl groups pointing either inward or outward. This was also tested within this study but was found to yield no difference in calculated T_1.

Introduction

Understanding cellulose supramolecular structure and the nature of its overall existing interfaces with water is important in many applications. For chemists working with cellulose, its reactivity is a crucial issue, and this is intimately connected to its interfacial properties.

In nature, cellulose is mainly found as slender fibrils where a precise number of glucan chains are organized in a parallel fashion. The lateral size of these fibrils, and consequently the number of its constituting glucan chains, depends on the synthesizing organisms. Extreme fibril lateral dimensions ranging from 2 to 20 nm have been reported in rare species, but the most common cellulose fibrils have diameters in the 3 to 5 nm region. Usually, these fibrils do not occur individually but are hierarchically assembled into bundles, herein referred to as fibril aggregates. Furthermore, the fibril aggregates themselves are organized into larger structures. The organization of the glucan chains within each cellulose fibril leads to a specific crystalline arrangement, defined as cellulose I or native cellulose, where all of the glucan chains are crystallized with their polar heads pointing in the same direction. Two crystalline cellulose I allomorphs have been identified, namely, the triclinic cellulose I α and the monoclinic I β, the former being dominant in some algal cell walls such as those of *Valonia* and the latter being the major constituent of higher plant cell walls such as those of cotton or wood, which will be considered here.

Solid-state cross-polarization magic angle spinning carbon-13 nuclear magnetic resonance (CP/MAS ^{13}C NMR) spectroscopy has been used during the last three decades to study cellulose.[2] It has for instance been used to identify the two coexisting crystalline allomorphs of native cellulose mentioned above, I α and I β.[3,4] The part of the spectrum that gives the highest apparent resolution is in the range 94−80 ppm where signals from C4 atoms are detected (see Figure 1D and Figure 2). Specifically, the resonance around 84 ppm has been proposed to originate from C4 atoms located at fibril surfaces.[5] This line has been further resolved into two relatively sharp peaks of equal intensity superimposed on a much broader signal.[6] One of a few proposed models for the fibril structure[7,8] is put forward by Larsson and Wickholm.[9,10] Following their nomenclature, fibril surfaces that constitute the envelope of fibril aggregates are hereafter referred to as accessible surfaces, whereas the remaining fibril surfaces, internal to the fibril aggregate, are referred to as inaccessible surfaces; these issues are clarified in Figure 1C. Within this model, the sharp peaks originate from accessible surfaces, whereas the broad peak comes from inaccessible surfaces. It might be worth noting that other models, especially those assuming different fibril cross sectional shapes, could provide other explanations for the broad signal. Furthermore, Larsson and Wickholm were able to measure different spin−lattice relaxation times T_1 for each peak, a procedure that has not been performed for any other atom in the cellulose

* Corresponding author. E-mail: malbe@kth.se.
† KTH Department of Fibre and Polymer Technology.
‡ STFI-Packforsk AB.
§ Centre de Recherches sur les Macromolécules Végétales.
|| E-mail: blund@kth.se.

10.1021/jp074641t CCC: $40.75
Published on Web 02/12/2008

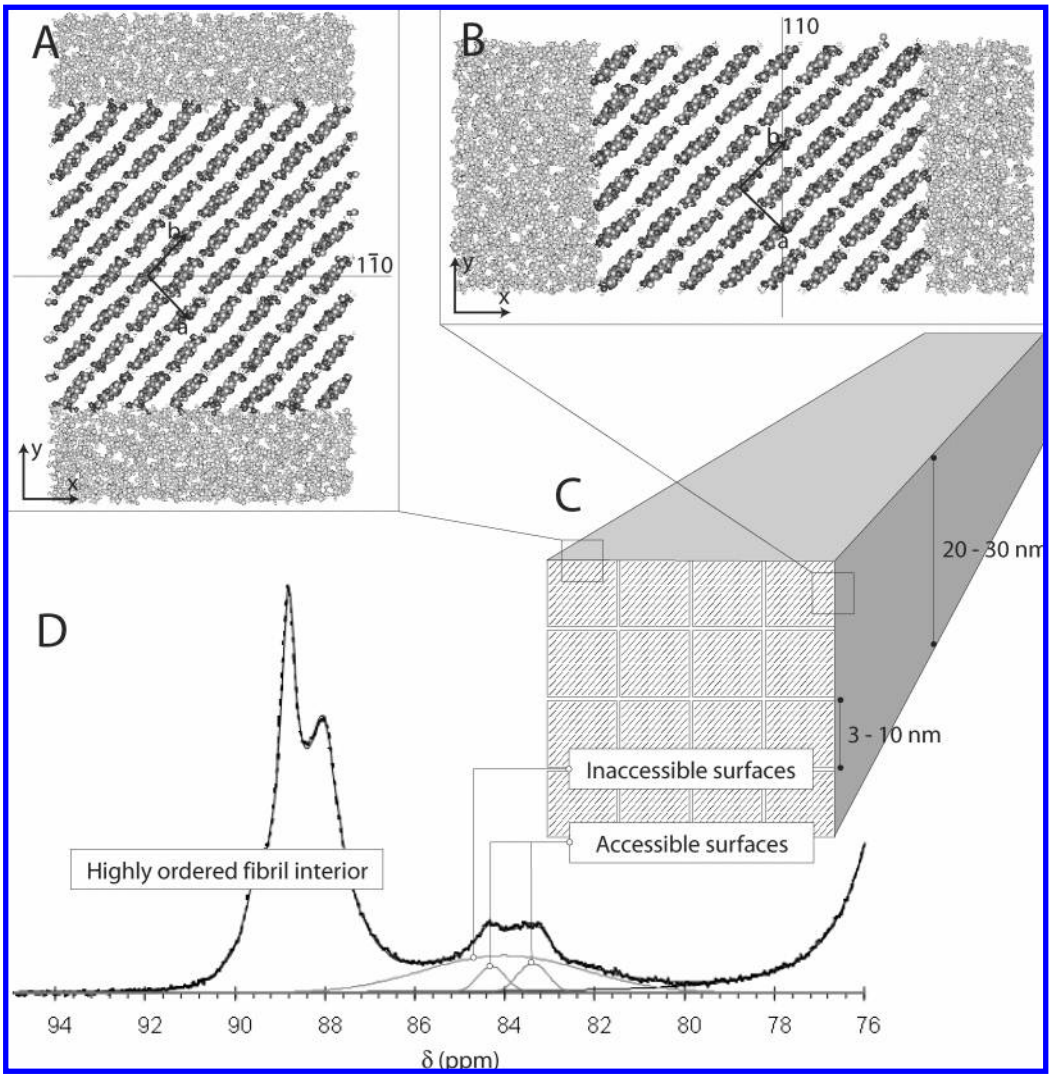

Figure 1. (A,B) Cellulose−water interfaces shown as snapshots from molecular dynamics simulations of the two system setups used in this work. The cellulose chain axis (*c*) is pointing out from the figure, making it parallel to the positive *z* axis. (C) Model for a fibril aggregate. Crystalline cellulose fibrils of typical dimension 3−10 nm assemble into aggregates of typical dimension 20−30 nm. The length of a fibril aggregate is much larger than its cross-sectional dimensions, of the order 0.1 μm or more. Fibril surfaces that constitute the envelope of the fibril aggregate are termed accessible surfaces. Fibril surfaces in the fibril aggregate interior are termed inaccessible surfaces. (D) CP/MAS ^{13}C NMR spectrum of C4 in hydrolyzed cotton linters (reproduced from ref 1). The large peak at 89 ppm is a collection of signals from the crystalline domains, whereas the broad peak at 84 ppm comes from noncrystalline regions. In this model, the latter is assumed to be a superposition of a broad signal from inaccessible surfaces and two signals from accessible surfaces.

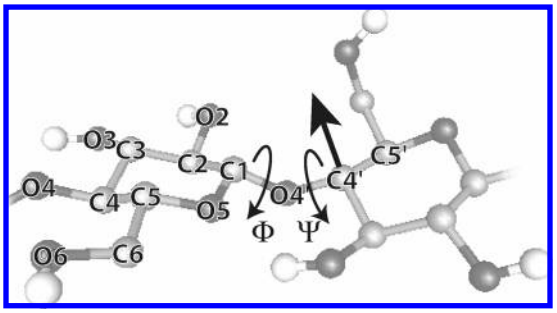

Figure 2. Cellobiosyl unit in cellulose. The model used is a united atoms model, which means that only polar hydrogens are explicitly included (white), while CH_x groups are modeled as single interaction sites (light gray). Oxygens are depicted dark. The direction of the C4−H4 bond, which can be calculated from the position of C4 and its bonded neighbors, are indicated by a large arrow. Furthermore, the definition of the torsional angles Φ (O5−C1−O4′−C4′) and Ψ (C1−O4′−C4′−C5′) are shown.

molecule. However, their model does not automatically explain why the signal from accessible surfaces would become a doublet. One proposed explanation for this is the nonequivalence of the anhydro-glucose units; half of them have hydroxymethyl groups protruding from the surface while the other half has hydroxymethyl groups pointing inward.[6]

Another reason could be a difference between surfaces that are parallel to different crystallographic planes.[10] Both suggestions are consistent with the observation that the integrated intensities under the two peaks are equal, but neither of them has yet been substantiated with experimental proof. Fortunately, the two signals for C4 yield different spin−lattice relaxation times, T_1, by almost a factor of 2,[10] a fact that makes it possible to approach the problem in another way, using computer modeling.

Molecular modeling has already been used to study bulk structures of cellulose.[11−19] Earlier computer modeling studies of cellulose−water interfaces[20,21] have shown that the cellulose structure at the surface is significantly different from the crystalline bulk structure. This is perhaps most evident in the distributions of the hydroxyl and hydroxymethyl torsional angles, which are strongly affected because of changes in the

hydrogen-bonding possibilities. These modeling studies do however suggest that the structural changes seem to affect only the outermost cellulose layer, while beneath that, the crystalline structure is preserved already in the second layer. The core of highly ordered fibrils may be crystalline, and two coexisting crystalline phases (I α and I β) may be simultaneously present. Each phase can form at least two nonequivalent surfaces, parallel to different underlying crystallographic planes. There are a few modeling studies concerned with the differences between the two cellulose I β surfaces.[21,22] They focus mainly on structural differences, which are found to be small.

The use of MD to study spin−lattice relaxation in partially ordered systems has been successful before in, for instance, lipid bilayers in the liquid crystalline phase.[23,24] It has never, to the authors' knowledge, been applied to crystalline cellulose, cellulose−water interfaces, or any system like it.

The objective for this present study is twofold. First, to provide the cellulose MD model with a relevant test by calculating spin−lattice relaxation times. This makes a direct comparison of its dynamics to experimental data possible. Partly due to limited availability of T_1 data in the literature, the present study deals only with relaxation of C4 atoms. Second, the question mentioned above regarding the double C4 surface signal in the NMR spectrum will be addressed. Spin−lattice relaxation will be examined separately for anhydro-glucose units in surface chains having their hydroxymethyl groups either pointing outward or inward, as well as for surface chains located on top of different crystallographic planes. Since higher plants are dominated by the I β phase, as mentioned earlier, we have restricted this study to the two most likely surfaces of cellulose I β, which are those being parallel to the (110) and ($1\bar{1}0$) crystallographic planes (see Figure 1A and B).

Theory

Assuming that the dominating relaxation mechanism for the C4 atom is spin−spin interaction between the ^{13}C nucleus and one attached proton, the ^{13}C spin−lattice relaxation time T_1 can be expressed as a linear combination of the spectral densities of some correlation function that describes the motion.[25,26] One particular choice is an autocorrelation function of the spherical harmonics, $Y_{2m}(\Omega)$, $\Omega = (\theta,\varphi)$, defining the direction of the C−H bond in spherical coordinates. This correlation function reads[23,26]

$$C_m(t) = \langle Y_{2m}(\Omega[t_0]) Y^*_{2m}(\Omega[t_0 + t]) \rangle_{t_0} \quad (1)$$

where the subscript t_0 means that the average is taken over all time origins. The spectral density is defined as

$$J_m(\omega) = \int_0^\infty C_m(t) \cos \omega t \, \mathrm{d}t \quad (2)$$

The heteronuclear spin−lattice relaxation time is related to the spectral density as

$$1/T_1 = \frac{4\pi}{10} \chi_0^2 [J_0(\omega_H - \omega_C) + 3J_1(\omega_C) + 6J_2(\omega_H + \omega_C)] \quad (3)$$

which, after careful rearrangment of prefactors, is identical to eq 2.6 of ref 26 and eq 2.3 of ref 23. This expression contains one frequency dependent part, which comes from the orientational dependence of the dipolar interaction. Here, ω_C and ω_H are the respective Larmor frequencies of the ^{13}C nucleus and the proton. The distance dependence is included in the constant of proportionality, which is the magnetic coupling constant. It is a combination of a few constants and the C−H bond distance r_{CH}, and it reads (in SI units)

$$\chi_0 = \left(\frac{\mu_0}{4\pi}\right) \frac{\gamma_C \gamma_H \hbar}{r_{CH}^3} \quad (4)$$

where μ_0 is the permeability of free space, γ_H and γ_C are the magnetogyric ratios of the nuclei (measured in rad s^{-1} T^{-1}), and $\hbar$ is Planck's constant divided by 2π.

In principle, a C4 nucleus will couple to every proton in the system. However, contributions from other protons than the one directly bonded to the C4 atom can safely be ignored since contributions to T_1 fall off extremely rapidly with distance. This is a consequence of the distance dependence in eq 3, where r_{CH} enters as the inverse of a sixth power.

Many experiments are performed under conditions where all orientations of the relevant C−H vectors relative to the magnetic field are equally probable. In constrast to a liquid, where rapid tumbling of the molecules causes loss of orientational correlation over fairly short periods of time, it is not motions of individual molecules that give rotational invariance in solid-state NMR. Instead, the rotational invariance originates in the disorder of molecules within the sample itself (e.g., a powder sample), so that the ensemble average of all vectors in the sample amounts to zero. Collective motions will of course be present, but these motions are assumed to appear on time scales much longer than the relaxation and thereby not to contribute to the spectral density at the frequencies of interest. With all orientations equally probable, the spectral density simplifies due to the addition theorem of the spherical harmonics[27] to

$$J_m(\omega) = \frac{j(\omega)}{4\pi} = \frac{1}{4\pi} \int_0^\infty C(t) \cos \omega t \, \mathrm{d}t \quad (5)$$

with

$$C(t) = \langle P_2(\cos\Delta[t_0, t_0 + t]) \rangle_{t_0} \quad (6)$$

Here, P_2 is the second-order Legendre polynomial and $\Delta[t_0,t_0 + t]$ is the angle between the C−H vectors at times t_0 and $t_0 + t$. Consequently, the expression for the relaxation rate simplifies to

$$1/T_1 = \frac{1}{10} \chi_0^2 [j(\omega_H - \omega_C) + 3j(\omega_C) + 6j(\omega_H + \omega_C)] \quad (7)$$

The numerical value of $(1/10)\chi_0^2$ is approximately 2×10^9 s^{-2}; it depends strongly on the exact value of r_{CH} which is assumed to be constant (1.08 Å).

Methods

Molecular dynamics simulations were performed using the GROMACS[28] simulation package.

The initial structure for crystalline cellulose I β was constructed from X-ray diffraction data,[29] and the force field was the GROMOS96 45A4 parameter set.[30] This particular model is described in detail elsewhere[31] and has been shown to provide good agreement with experimental data at room temperature for the bulk structure, Young's modulus, and thermal response. For the water, the SPC model[32] was employed.

Two different systems were used in this study, hereby referred to as system A and system B (see Figure 1). Both comprised crystalline cellulose I β and water in a fully periodic box, representing an accessible fibril surface, but with some small differences. System A consisted of 8×8 glucan chains giving

a cross section of 4.6 nm × 4.7 nm and 1802 water molecules giving a water layer 2.8 nm thick. In this system, the cellulose−water interfaces were parallel to the $(1\bar{1}0)$ crystallographic plane. The two surfaces in system A are equivalent and will be referred to as type A surfaces throughout the text. The other system, B, consisted of 8 × 6 chains (4.6 nm × 3.5 nm) and 1773 water molecules (3.7 nm), with interfaces parallel to the (110) plane. Consequently, these surfaces will be referred to as type B surfaces. In both systems, the chains consisted of 8 anhydroglucose units, with a total length of approximately 4.2 nm. Each chain was covalently bonded to its own periodic image, mimicking chains of infinite length.

Pressure was kept constant at 1 atm using the Berendsen algorithm,[33] and a temperature of 293 K was maintained with a Nosé−Hoover thermostat.[34,35]

The simulations used the Leapfrog algorithm with a time step of 1 fs. A cutoff of 1 nm was used for the nonbonded interactions, but long-range contributions were included by PME[36,37] for electrostatics and an analytical dispersion correction for Lennard-Jones interactions. Bonds were kept rigid throughout the whole simulation using LINCS[38] for cellulose and SETTLE[39] for water. After equilibration, simulations were extended for 5 ns each.

Results and Discussion

Rotational Autocorrelation Functions. Since the present model uses united atoms, there is no explicit hydrogen on the C4 atom. Its position can however be calculated from the position of C4 and its covalently bonded neighbors, assuming perfect tetrahedal symmetry (see Figure 2). This was done using coordinates stored every ps from the simulations, and rotational autocorrelation functions of the C4−H4 bond vectors were calculated according to eq 6. All C4 atoms in surface chains were used in the calculations, amounting to 128 for type A surfaces and 96 for type B, and their autocorrelations were calculated independently. Motions of the C−H bond vectors are obviously restricted in space. This means that rotational autocorrelation functions do not fall off to zero but to a constant value S^2 which is interpreted as an order parameter. Calculated autocorrelation functions, $\tilde{C}(t)$, were scaled according to $C(t) = (\tilde{C}(t) - S^2)/(\tilde{C}(0) - S^2)$ which leaves only correlations of the fluctuations. For both surfaces, the (squared) order parameter was calculated to $S^2 = 0.94$.

C4 Atoms in the Fibril Interior. The autocorrelation functions for C4−H4 vectors in the fibril interior decay rapidly to zero, on time scales much shorter than 1 ps. From our simulation data, we cannot make any reliable statements about their functional form, nor are we able to discriminate between different crystalline layers. This observation might be important regarding a discussion on the existence of a paracrystalline or subcrystalline layer located just underneath accessible surfaces.[2,8,10] Our simulations do not provide any evidence for this hypothesis, nor do they disprove it.

C4 Atoms at Fibril Surfaces. The main decay of $C(t)$ at surfaces takes place at a time scale of a few picoseconds, but there is also an additional long-time tail that persists out to, at least, several hundred picoseconds (Figure 3).

In our model, the large difference between anhydro-glucose units that have their hydroxymethyl groups pointing either outward or inward is the conformation of the torsional angle ω (O5−C5−C6−O6 in Figure 2). The hydroxymethyl group has three staggered conformations usually labeled tg ($\omega = 180°$), gg ($\omega = 300°$), and gt ($\omega = 60°$), respectively. The inward-pointing groups are without exception locked in a tg conformation which is consistent with experimental findings for the crystal structure.[29] Groups pointing out from the surface on the other hand are found in either gg or gt, with a preference for gg. This is also consistent with experiments.[40] Our calculations however showed no difference in $C(t)$ between these two situations, which implies that the conformation of ω has no effect on the C4−H4 dynamics.

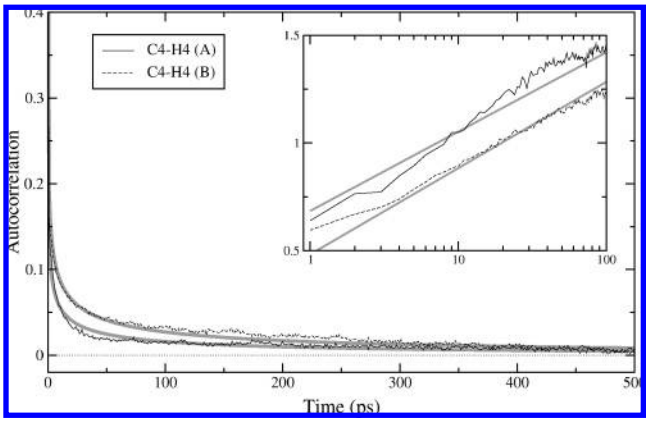

Figure 3. Rotational autocorrelation functions, $C(t)$, for C4−H4 vectors belonging to surfaces of type A (solid black) and B (dashed). The solid gray curves are fits of stretched exponential functions. The parameters used are for A, $\tau = 0.0139$ ps and $\alpha = 0.160$ and for B, $\tau = 0.0625$ ps and $\alpha = 0.174$. In a plot of log [−log[$C(t)$]] versus log(t), stretched exponentials show up as straight lines (inset).

In contrast, and importantly, there was an obvious difference between decays in surface chains located on top of different crystallographic planes. Autocorrelation functions for chains belonging to type A surfaces, and hence parallel to $(1\bar{1}0)$ decayed faster than for chains in type B surfaces, parallel to (110). This observation will be a main theme for the remainder of this text.

The decay of $C(t)$ could not be fitted with a single-exponential function with just one correlation time. This was to be expected, since the dynamics take place in a very complex energy landscape, defined by several angle and torsion angle potentials as well as nonbonded interactions with both water and neighboring cellulose chains.

There are several different possibilities to describe the functional form of this kind of decay. One way would be to use a weighted sum of a finite number of exponential functions with different correlation times. Another possibility is to use algebraic decays, $C(t) \propto t^{-\alpha}$, although they diverge at $t = 0$. A third choice is the often used stretched exponential function (or Kohlrausch−Williams−Watts function), $C(t) = \exp\{-(t/\tau)^{\beta}\}$. In the end, the result proved to be independent of which analytical form was used for the fit, which gives an indication of the robustness of our calculations. For the rest of the analysis presented here, stretched exponential functions are used which is the best choice in our opinion. The physical interpretation of the stretched exponential function is that it is a sum of single-exponential functions, $\exp\{-(t/\tau)^{\beta}\} = \int_0^{\infty} \exp\{-t/\tau\}\ \rho(\tau)\ d\tau$, where $\rho(\tau)$ is a distribution of correlation times. However, in contrast to a finite sum, the stretched exponential function depends on two parameters only, τ and β, a fact that makes it convenient for fitting purposes. See, for example, refs 40−43 for discussions on these functions and their applicability. Stretched exponential functions fitted to the calculated $C(t)$, using least-square fits to data out to 1 ns, are displayed in Figure 3.

Spin−Lattice Relaxation Times. Spectral densities, $j(\omega)$, were calculated using the numerical fast Fourier transform (FFT)

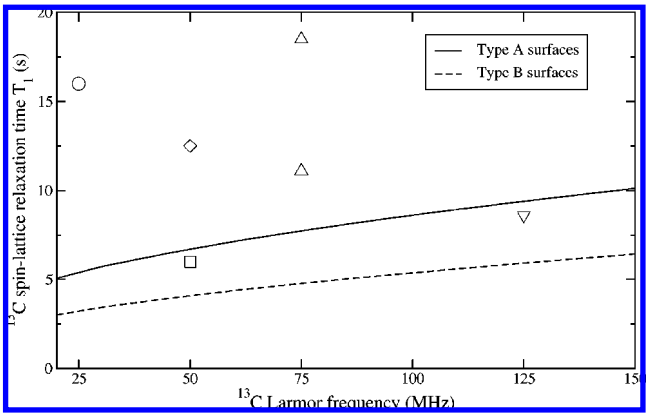

Figure 4. ^{13}C spin−lattice relaxation times as function of carbon Larmor frequency. Calculated values for the two surfaces A (solid) and B (dashed) are compared to experimental points from (◇) Horii et al.[45] and Teeäär and Lippmaa,[46] (□) Newman et al.,[47] (○) Love et al.,[48] (▽) Kristensen et al.,[49] and (△) Wickholm et al. ,[10] which is the only experiment that reports two separate T_1.

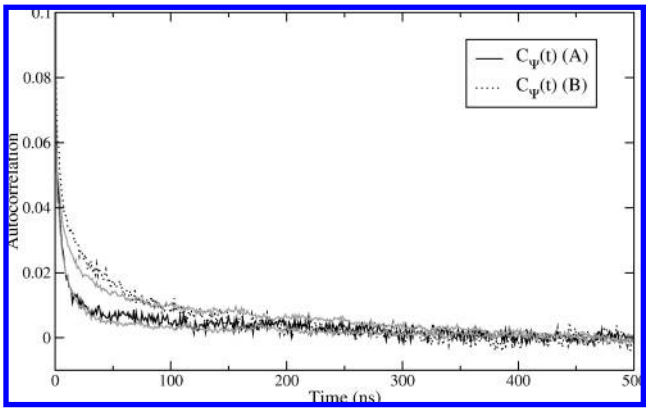

Figure 5. Autocorrelation functions for the torsional angle Ψ. Solid line refers to surface A and dashed to surface B. Light gray lines are rotational autocorrelation functions from Figure 3. They are scaled with the same factor to fall on the angular autocorrelation functions, which serves to show that they exhibit similar differences between surfaces of types A and B.

on the fitted stretched exponential functions, which unfortunately lack an analytical transform. It would in principle be possible to use calculated autocorrelation functions directly and calculate spectral densities by applying FFT's on raw data. In practice though, this would require very long simulations, and therefore, it was not feasible because of computational limitations.

As a final step, spin−lattice relaxation times T_1 were calculated as linear combinations of spectral densities, according to eq 7. This was done for the surfaces of types A and B separately, and the resulting curves, T_1 as function of Larmor frequency, are displayed in Figure 4 along with some experimental points. Please note that there exists only one experiment that assigns two separate T_1 to the C4 surface signal[10] (triangles at 75 MHz). Provided this assignment is correct, the other values can be regarded as averages. There are several important observations that can be made regarding Figure 4.

Both experimental and calculated T_1 fall within 1 order of magnitude, 3−20 s, for the whole frequency range. The calculated values might be on the low side, which would mean that the dynamics in this model is slightly slower compared to experimental results.

The difference between calculated spin−lattice relaxation times for surfaces of types A and B (7.7 and 4.8 s) is a factor 1.6 at 75 MHz. This matches the ratio between 18.5 and 11.1 s from Wickholm et al.[10] From a spectroscopist's point of view, it might be of interest to notify that we therewith are able to assign the different signals in the doublet around 84 ppm to surfaces parallel to different crystallographic planes. The signal at 84.3 ppm belongs to surfaces parallel to $(1\bar{1}0)$ and the one at 83.4 belongs to surfaces parallel to (110).

It is the difference in area under the curves in Figure 3 that gives rise to different calculated relaxation times, with the slower decay of $C(t)$ for type B surfaces leading to a shorter T_1.

Reasons for the Difference between Type A and Type B Surfaces. Surfaces of types A and B do not differ in an obvious way, perhaps with the exception of having slightly different interchain repeat distances. The average distance between chains in our model is 0.578 nm for type A surfaces and 0.590 nm for type B. This is surely not a big difference, only about one tenth of an angstrom, but the question is if that is enough to cause the difference in relaxation. Furthermore, this becomes an important issue since our simulated spacings differ slightly from the experimental values[29] of 0.581 and 0.596 nm, respectively. However, additional simulations were performed. The box sides were there constrained to give the larger spacing 0.590 nm for type A surfaces and the smaller 0.578 nm for type B surfaces. These simulations showed no significant difference in relaxation behavior when compared to the original simulations.

Our simulations, as well as earlier modeling studies,[21,22] show that the surfaces are structurally very similar; differences in density profiles and radial distribution functions are small. However, in a recent study Matthews et al.[17] found a small difference between preferred conformations of ω in (110) and $(1\bar{1}0)$ surfaces respectively. If this was indeed the case in a real fibril, it could explain the difference in chemical shift of C4 between the surfaces but would probably not be the underlying cause for differences in relaxation (see above). In our simulations, distributions of torsional angles for side-groups are the same for both surfaces, but bearing in mind that this property is extremely sensitive to model parameters, we cannot rule out this possibility altogether.

The torsional angles Φ and Ψ (defined in Figure 2) that describe the conformation of the glucosidic linkage in the cellulose chain are of specific interest since they affect the direction of the C4−H4 vector in a direct manner. However, attempts to correlate these angles to the C4 chemical shift has not been successful,[50] and our simulations gave no significant difference in angular distributions for Φ and Ψ between type A and type B surfaces, or even compared to the crystalline interior. But where we failed to correlate structural properties to the dynamics of the C4−H4 vectors, we did see a striking similarity in dynamical properties.

Dihedral autocorrelation functions $C_\Psi(t) = \langle \cos(\Psi(t_0) - \Psi(t_0 + t)) \rangle_{t_0}$ calculated for chains belonging to the two surface types are shown in Figure 5. Since $C_\Phi(t)$ looks the same, it is not included in the figure. Apparently, the dihedral dynamics in type B surfaces are slower than in type A surfaces, which shows up as a longer tail in its autocorrelation function, in a similar way as for $C(t)$. By scaling the autocorrelation functions from Figure 3 with a single factor, they were made to fall approximately onto the dihedral autocorrelation functions in Figure 5. In general, $C(t)$ and $C_\Psi(t)$ are not necessarily directly comparable, but this operation serves to show that the same difference between the surfaces of type A and type B that was found for the C4−H4 vector dynamics is present in the Ψ and Φ dihedral dynamics as well. In addition, dihedral autocorrelation functions for Ψ and Φ in the crystalline interior fall off to zero on very short times (not shown).

Looking at the cellulose structure in Figure 2, we find it is not hard to realize how the C4−H4 bond is intimately connected to the glucosidic dihedral angles. We also note that autocorrelation functions for other torsional angles, for example, those within glucose rings, do not exhibit any measurable differences between surface types. The appropriate interpretation must be that the difference in C4−H4 vector dynamics between the surfaces, and thus the difference in spin−lattice relaxation times, is a direct consequence of the dynamics of the glucosidic torsional angles, with surfaces of type A having stiffer links than type B surfaces.

Conclusions

For the first time, molecular dynamics simulations of cellulose have been compared to spin−lattice relaxation times, T_1, from solid-state CP/MAS ^{13}C NMR. Calculated T_1 values for C4 atoms in surface chains at cellulose−water interfaces are in good agreement with available experimental data, meaning that the present force field reproduces relevant surface dynamics at a sufficiently high level.

It was found that the calculated T_1 was larger by a factor of 1.6 for C4 atoms located in surfaces parallel to the $(1\bar{1}0)$ crystallographic plane (called type A surfaces within this paper), as compared with surfaces parallel to (110) (type B surfaces). This result reproduces the experimentally observed difference between T_1 values for the two sharp C4 signals at 84 ppm, and thus lends support to the interpretation that the reason for this doublet is nonequivalence of accessible surfaces located on top of different crystallographic planes.

The spin−lattice relaxation is found to be intimately connected to the flexibility of the glucosidic linkage. Autocorrelation functions for the dihedral angles Φ and Ψ decay faster in type A surfaces than in type B surfaces, which has a direct influence on the rotational autocorrelation function for the C4−H4 vector.

Why this difference in backbone dynamics between surfaces exists, we presently cannot answer in a satisfactory manner. It was found that the difference between interchain repeat distances of the two surfaces under study is not of consequence, and other observed structural differences were deemed too small to be of any practical importance.

The understanding of cellulose surface properties is not complete, and interpretations of its NMR spectrum are ambiguous. We have shown that atomistic computer simulations, in close collaboration with experiments, have the potential to shed light on these matters.

Financial support from the centers BiMaC and BioMime at KTH is gratefully acknowledged (L.B. and M.B.). The authors are grateful to Olle Edholm for granting computer time on his PC cluster.

References and Notes

(1) Larsson, P. T.; Westlund, P.-O. *Specrochim. Acta A* **2005**, *62*, 539−546.
(2) Atalla, R. H.; VanderHart, D. L. *Solid State Nucl. Magn. Reson.* **1999**, *15*, 1−19.
(3) Atalla, R. H.; VanderHart, D. L. *Science* **1984**, *223*, 283−285.
(4) VanderHart, D. L.; Atalla, R. H. *Macromolecules* **1984**, *17*, 1465−1472.
(5) Earl, W. L.; VanderHart, D. L. *Macromolecules* **1981**, *14*, 570−574.
(6) Newman, R. H.; Hemmingson, J. A. *Cellulose* **1995**, *2*, 95−110.
(7) Brown, R. M., Jr. *J. Polym. Sci., Polym. Chem.* **2004**, *42*, 487−495.
(8) Ding, S.-Y.; Himmel, M. E. *J. Agric. Food Chem.* **2006**, *54*, 597−606.
(9) Larsson, P. T.; Wickholm, K.; Iversen, T. *Carbohydr. Res.* **1997**, *302*, 19−25.
(10) Wickholm, K.; Larsson, P. T.; Iversen, T. *Carbohyd. Res.* **1998**, *312*, 123−129.
(11) French, A. D.; Miller, D. P.; Aablo, A. *Int. J. Biol. Macromol.* **1993**, *15*, 30−36.
(12) Aablo, A.; French, A. D. *Macromol. Theory Simul.* **1994**, *3*, 185−191.
(13) Aablo, A.; French, A. D.; Mikelsaar, R.-H.; Pertsin, A. J. *Cellulose* **1994**, *1*, 161−168.
(14) Neyertz, S.; Pizzi, A.; Merlin, A.; Maigret, B.; Brown, D.; Deglise, X. *J. Appl. Polym. Sci.* **2000**, *78*, 1939−1946.
(15) Mazeau, K.; Heux, L. *J. Phys. Chem. B* **2003**, *107*, 2394−2403.
(16) Tanaka, F.; Okamura, K. *Cellulose* **2005**, *12*, 243−252.
(17) Matthews, J. F.; Skopec, C. E.; Mason, P. E.; Zuccato, P.; Torget, R. W.; Sugiyama, J. *Carbohydr. Res.* **2005**, *341*, 138−152.
(18) Yui, T.; Nishimura, S.; Akiba, S.; Hayashi, S. *Carbohydr. Res.* **2006**, *341*, 2521−2530.
(19) Yui, T.; Hayashi, S. *Biomacromolecules* **2007**, *8*, 817−824.
(20) Heiner, A. P.; Teleman, O. *Langmuir* **1997**, *13*, 511−518.
(21) Heiner, A. P.; Kuutti, L.; Teleman, O. *Carbohyd. Res.* **1998**, *306*, 205−220.
(22) Biermann, O.; Hädicke, E.; Koltzenburg, S.; Müller-Plathe, F. *Angew. Chem., Int. Ed.* **2001**, *40*, 3822−3825.
(23) Lindahl, E.; Edholm, O. *J. Chem. Phys.* **2001**, *115*, 4938−4950.
(24) Wohlert, J.; Edholm, O. *J. Chem. Phys.* **2006**, *125*, 204703.
(25) Abragam, A. *The principles of nuclear magnetism;* Oxford University Press: Amen House London E.C.4, 1961.
(26) Brown, M. F. *J. Chem. Phys.* **1984**, *80*, 2808−2830.
(27) Arfken, G. B.; Weber, H. J. *Mathematical methods for physicists*, 4th ed.; Academic Press: San Diego, 1995.
(28) van der Spoel, D.; Lindahl, E.; Hess, B.; Groenhof, G.; Mark, A. E.; Berendsen, H. J. C. *J. Comput. Chem.* **2005**, *26*, 1701−1718.
(29) Nishiyama, Y.; Langan, P.; Chanzy, H. *J. Am. Chem. Soc.* **2002**, *124*, 9074−9082.
(30) Lins, R. D.; Hünenberger, P. H. *J. Comput. Chem.* **2005**, *26*, 1400−1412.
(31) Bergenstråhle, M.; Berglund, L.; Mazeau, K. *J. Phys. Chem. B* **2007**, *111*, 9138−9145.
(32) Berendsen, H. J. C.; Postma, J. P. M.; van Gunsteren, W. F.; Hermans, J. *Intermolecular Forces*; Pullman, B., Ed.; Riedel: Dordrecht, The Netherlands, 1981.
(33) Berendsen, H. J. C.; Postma, J. P. M.; van Gunsteren, W. F.; DiNola, A.; Haak, J. R. *J. Chem. Phys.* **1984**, *81*, 3684−3690.
(34) Nosé, S. *Mol. Phys.* **1984**, *55*, 255−268.
(35) Hoover, W. G. *Phys. Rev. A* **1985**, *31*, 1695−1697.
(36) Darden, T.; York, D.; Pedersen, L. G. *J. Chem. Phys.* **1993**, *98*, 10089−10092.
(37) Essmann, U.; Perera, L.; Berkowitz, M. L.; Darden, T.; Lee, H.; Pedersen, L. G. *J. Chem. Phys.* **1995**, *103*, 8577−8593.
(38) Hess, B.; Bekker, H.; Berendsen, H. J. C.; Fraaije, J. G. E. M. *J. Comput. Chem.* **1997**, *18*, 1463−1472.
(39) Miyamoto, S.; Kollman, P. A. *J. Comput. Chem.* **1992**, *13*, 952−962.
(40) Newman, R. H.; Davidson, T. C. *Cellulose* **2004**, *11*, 23−32.
(41) Williams, G.; Watts, D. C. *Trans. Faraday Soc.* **1970**, *66*, 80−85.
(42) Linidsey, C. P.; Patterson, G. D. *J. Chem. Phys.* **1980**, *73*, 3348−3357.
(43) Alvarez, F.; Alegra, A.; Colmenero, J. *Phys. Rev. B* **1991**, *44*, 7306−7312.
(44) Edholm, O.; Blomberg, C. *Chem. Phys.* **2000**, *252*, 221−225.
(45) Horii, F.; Hirai, A.; Kitamaru, R. *The structures of cellulose*; Atalla, R. H., Ed.; American Chemical Society: Washington DC, 1987; Chapter 6, pp 119−134.
(46) Teeäär, R.; Lippmaa, E. *Polymer Bull.* **1984**, *12*, 315−318.
(47) Newman, R. H.; Davies, L. M.; Harris, P. J. *Plant Physiol.* **1996**, *111*, 475−485.
(48) Love, G. D.; Snape, C. E.; Jarvis, M. C. *Phytochemistry* **1998**, *49*, 1191−1194.
(49) Kristensen, J. H.; Bampos, N.; Duer, M. *Phys. Chem. Chem. Phys.* **2004**, *6*, 3175−3183.
(50) Jarvis, M. C. *Carbohydr. Res.* **1994**, *259*, 311−318.